

Intrinsic viscosity of a suspension of weakly Brownian ellipsoids in shear

G. Almondo^{*1}, J. Einarsson^{*1}, J. R. Angilella², B. Mehlig¹

¹*Department of Physics, University of Gothenburg, 41296 Gothenburg, Sweden. and*

²*Université de Caen, Cherbourg, France.*

*These authors contributed equally to this work.

(Dated: June 14, 2018)

We analyze the angular dynamics of triaxial ellipsoids in a shear flow subject to weak thermal noise. By numerically integrating an overdamped angular Langevin equation, we find the steady angular probability distribution for a range of triaxial particle shapes. From this distribution we compute the intrinsic viscosity of a dilute suspension of triaxial particles. We determine how the viscosity depends on particle shape in the limit of weak thermal noise. While the deterministic angular dynamics depends very sensitively on particle shape, we find that the shape dependence of the intrinsic viscosity is weaker, in general, and that suspensions of rod-like particles are the most sensitive to breaking of axisymmetry. The intrinsic viscosity of a dilute suspension of triaxial particles is smaller than that of a suspension of axisymmetric particles with the same volume, and the same ratio of major to minor axis lengths.

I. INTRODUCTION

Einstein [1, 2] calculated the shear viscosity μ^* of a dilute suspension of non-interacting spheres in a viscous fluid. He found $\mu^* = \mu(1 + \eta\phi)$, where μ is the viscosity of the suspending fluid, $\eta = 5/2$ is the *intrinsic viscosity*, and ϕ is the concentration by volume of the suspended spheres. The suspension viscosity is larger than that of the suspending fluid because the particle cannot deform as the suspension is sheared. There is extra stress in the particle to resist the surface traction from the flow, and therefore there is a contribution proportional to the volume fraction of particles [3].

For a non-spherical particle, this additional stress depends on the orientation of the particle relative to the shear flow, and it also depends upon the particle shape. Jeffery [4] calculated the angular motion and dissipation for a small ellipsoidal particle in order to determine the intrinsic viscosity η for a dilute suspension of ellipsoids. He found that the angular motion, and consequently the intrinsic viscosity, depends indefinitely on the initial orientation of the ellipsoid. This indeterminacy is physically unsatisfactory because the macroscopic suspension viscosity μ^* should not depend on the detailed microscopic initial conditions of the suspended particles after a long time.

For larger particles, the effects of inertia may break this indeterminacy [4–10]. But the long-time dynamics still depends on the initial condition for sufficiently flat disk-shaped particles [9], which could lead to hysteresis in the rheological functions of an inertial suspension.

For small particles, thermal fluctuations render the particle trajectories stochastic, and eventually independent of their initial conditions. In this case the intrinsic viscosity η is a function of particle shape and noise strength, when averaged over an ensemble of stochastic realizations [11, 12]. For spheroidal particles subject to sufficiently weak noise, the stationary angular distribution is independent of noise strength [12, 13]. This is because the angular dynamics is well described by the deterministic Jeffery trajectories in this limit, but with occasional jumps to a nearby trajectory. After many such jumps, a stationary probability distribution over the deterministic trajectories is established, however, the time to reach equilibrium is longer for weaker noise strength. The dilute, weak-noise rheology is given by averaging over this stationary distribution. The intrinsic viscosity of a suspension of spheroids is larger than that of a suspension of spheres, and the shape dependence is stronger for prolate spheroids than oblate spheroids [12].

How do these results generalize to triaxial ellipsoids? Much less is known concerning particles that do not possess axisymmetry. In absence of noise, the angular trajectory of a triaxial ellipsoid in shear flow is doubly periodic or chaotic, but nevertheless depends indefinitely upon initial condition [14–17]. Similarly to the case of axisymmetric ellipsoids, thermal fluctuations eventually establish a stationary distribution over these trajectories, and this angular distribution determines the suspension rheology. For strong noise Rallison [18] and Haber and Brenner [19] determined the first deviations from the uniformly distributed equilibrium state. But the angular distributions and the resulting intrinsic viscosity in the weak noise regime remain unknown. It is hard to make analytical progress, because the deterministic dynamics is chaotic.

In this paper we numerically compute the angular distribution and resulting intrinsic viscosity for a range of triaxial ellipsoids in shear flow, subject to weak thermal noise. We derive the appropriate Langevin equation and solve it numerically for the stationary probability distribution. We show how the angular distribution reflects the underlying deterministic trajectories. We compute the resulting intrinsic viscosity for a dilute suspension and show that it is maximal for axisymmetric particle shapes. In general the shape dependence of the intrinsic viscosity is weaker than that of the deterministic angular dynamics, which depends very sensitively on particle shape.

The remainder of this paper is organized as follows. In Section II we present our notation, derive the Langevin equation, and give the relation between the angular distribution and the dilute suspension viscosity. Section III contains the numerical results from our Langevin simulations. We discuss the results in Section IV and conclude in Section V.

II. THEORY

A. Notation

Where possible we use vector notation without indices. We write vectors as \mathbf{a} , and their components in the lab frame as a_i . Tensors are denoted by \mathbb{A} , and $A_{ij\dots}$ are the lab-frame components of this tensor. In some instances we find index notation necessary for clarity, and then we use the Einstein summation convention. Contractions of adjacent indices are denoted by the dot product, as for example in the scalar product between two vectors $\mathbf{a} \cdot \mathbf{b} = a_i b_i$. The double dot product denotes contraction of two adjacent indices. For example, $(\mathbb{A} : \mathbb{B})_{il} = A_{ijk} B_{kjl}$ denotes a contraction between the two rank-3 tensors \mathbb{A} and \mathbb{B} . These conventions apply also to contractions between tensors of different ranks.

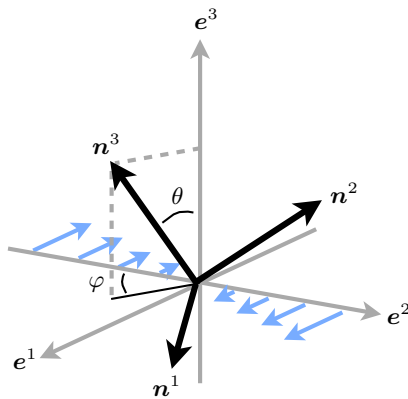


FIG. 1. Coordinate system. Flow direction e^1 , shear direction e^2 . The flow vorticity points along $-e^3$. The angle between the principal axis n^3 and the e^3 -axis is θ , and φ is the angle between the $-e^2$ -axis and the projection of n^3 onto the flow-shear plane. See appendix A for details concerning the definition of the angles.

We represent the shape and orientation of an ellipsoid by the lengths (a_1, a_2, a_3) and directions (n^1, n^2, n^3) of its principal semi-axes. Without loss of generality we take $a_1 \leq a_2 \leq a_3$. The two aspect ratios are $\lambda = a_3/a_1$ and $\kappa = a_2/a_1$. We denote the coordinate axes of the lab frame by (e^1, e^2, e^3) . They are fixed with respect to the undisturbed fluid flow. The undisturbed flow takes the form $\mathbf{u}^\infty = \boldsymbol{\Omega}^\infty \times \mathbf{r} + \mathbb{E}^\infty \cdot \mathbf{r}$ where \mathbf{r} is the spatial coordinate vector, $\boldsymbol{\Omega}^\infty$ is half the fluid vorticity, and \mathbb{E}^∞ is the strain-rate matrix of the flow. We take the undisturbed flow to be a simple shear, $\mathbf{u}^\infty = (sr_2, 0, 0)$, as shown in Fig. 1.

We also use the convention that components of a tensor in the particle coordinate frame have Greek indices, while components in the fixed lab frame have Latin indices, for example

$$\mathbf{X} = \sum_{i=1}^3 X_i \mathbf{e}^i = \sum_{\alpha=1}^3 X_\alpha \mathbf{n}^\alpha. \quad (1)$$

The two sets of components are related by the matrix \mathbb{R} , defined by $\mathbf{e}^i = \mathbb{R} \mathbf{n}^i$, so that

$$X_\alpha = R_{\alpha i} X_i, \quad X_i = R_{i\alpha}^\top X_\alpha. \quad (2)$$

Here $R_{i\alpha}^\top$ are the elements of \mathbb{R}^\top , the transpose of \mathbb{R} . Since the bases \mathbf{e}^i and \mathbf{n}^α are both orthonormal, \mathbb{R} is orthogonal, so that $\mathbb{R}^{-1} = \mathbb{R}^\top$. Appendix A explains how the elements of \mathbb{R} are expressed in terms of Euler angles [20]. The components of the particle-orientation vector \mathbf{n}^β in the lab frame are given by

$$n_i^\beta = R_{i\alpha}^\top n_\alpha^\beta = R_{\beta i}. \quad (3)$$

In the remainder of this paper we employ dimensionless variables. We scale length by $V_p^{1/3}$ and time by $1/s$, where V_p is the volume of the particle, and s is the magnitude of the undisturbed shear rate. Stress is scaled by μs , where μ is the viscosity of the suspending fluid.

B. Orientational dynamics

Disregarding thermal noise, the hydrodynamic angular velocity of an ellipsoidal particle in a linear Stokes flow $\mathbf{u}^\infty = \boldsymbol{\Omega}^\infty \times \mathbf{r} + \mathbb{E}^\infty \cdot \mathbf{r}$ is given by

$$\boldsymbol{\omega}^H = \boldsymbol{\Omega}^\infty + \mathbb{K}^{-1} \cdot \mathbb{H} : \mathbb{E}^\infty. \quad (4)$$

The resistance tensors \mathbb{K} and \mathbb{H} are given by Haber and Brenner [19] (see Table I for translation of notation). The tensor \mathbb{K} describes the viscous resistance against a steady rotation of the particle, while \mathbb{H} determines the effect of fluid strain on the hydrodynamic torque. The components of the resistance tensors are constant when expressed in the body frame, conversely the components of the flow gradients ($\boldsymbol{\Omega}^\infty$ and \mathbb{E}^∞) are constant when expressed in the fixed lab frame. Therefore the components of the angular velocity, either in the body or the lab frame, depend on the orientation of the particle.

Thermal fluctuations randomize the particle orientation. The resulting angular probability distribution $P(\mathbb{R}, t)$ is governed by the Fokker-Planck equation [18, 19, 21]

$$\frac{\partial P}{\partial t} + \nabla \cdot (\boldsymbol{\omega}^H - \text{Pe}^{-1} \mathbb{D} \cdot \nabla) P = 0. \quad (5)$$

Here $\text{Pe} = \mu V_p s / (k_B T)$ is the Péclet number which is a dimensionless measure of the noise strength. The non-dimensional diffusion tensor is given by $\mathbb{D} = \mathbb{K}^{-1}$. A corresponding relation for the centre-of-mass diffusion of a small particle was first deduced by Einstein [1, 2]. In the steady state the diffusion flux must equal the flux due to the external force, resulting in the relation $D = k_B T / (\mu V_p)$ for the dimensional rotational diffusion constant (which has the units of inverse of time). Einstein's argument was adapted to the rotation of triaxial ellipsoids by Perrin [22], and leads directly to Eq. (5): the first term in the parentheses on the l.h.s. of this equation is the angular flux due to the imposed flow, a shear in our case. The second term is the angular diffusion flux. Our notation is closest to that of Rallison [18] who studied this equation in the limit of strong noise. The gradients in the Fokker-Planck equation (5) have the components $\nabla_k = \varepsilon_{kij} R_{\alpha i} \partial_{\alpha j}$ where $\partial_{\alpha j}$ is the unconstrained differential in the nine-dimensional space of linear transformations [18], and ε_{kij} is the Levi-Civita symbol denoting the elements of the completely antisymmetric third-rank tensor.

We do not solve Eq. (5) directly. Instead we consider the equivalent Langevin equation [21, 23] for the angular increments $\delta \mathbb{R}$ during the time interval δt :

$$\mathbb{R}(t + \delta t) = \mathbb{R}(t) + \delta \mathbb{R}(t), \quad (6a)$$

$$\overline{\delta R_{\alpha i}} = -\varepsilon_{\alpha\beta\gamma} \omega_{\beta}^H(t) R_{\gamma i}(t) \delta t + \text{Pe}^{-1} \varepsilon_{\alpha\beta\gamma} \varepsilon_{\gamma\rho\sigma} K_{\beta\rho}^{-1} R_{\sigma i}(t) \delta t, \quad (6b)$$

$$\overline{\delta R_{\alpha i} \delta R_{\mu p}} = 2\text{Pe}^{-1} \varepsilon_{\alpha\beta\gamma} \varepsilon_{\mu\rho\sigma} R_{\gamma i}(t) R_{\sigma p}(t) K_{\beta\rho}^{-1} \delta t. \quad (6c)$$

In the limit of weak noise, Eqs. (6) are valid provided that $\text{St} \ll \delta t \ll 1$. The lower limit for δt is given by the Stokes number $\text{St} = \rho_p s V_p^{2/3} / \mu$, a dimensionless measure of the particle inertia, where ρ_p is the particle density. We must assume that the Stokes number is small enough so that the condition on δt can be satisfied. In this paper we consider the limit of large (but finite) Péclet numbers. In this case the upper limit for δt is determined by the shear rate, so it is equal to unity in our dimensionless variables. In Eq. (6b) and (6c) the over-bar denotes an average over fluctuating angular displacements at fixed initial particle orientations, distinct from the thermal average $\langle \dots \rangle$ over the steady-state distribution of orientations.

The Langevin equation (6) can be derived directly from the angular-momentum equation [21]

$$\begin{aligned} \text{St} \frac{d(\mathbb{I}\boldsymbol{\omega})}{dt} &= \mathbb{K} \cdot (\boldsymbol{\Omega}^\infty - \boldsymbol{\omega}) + \mathbb{H} : \mathbb{E}^\infty + \boldsymbol{\Gamma}(t), \\ \langle \boldsymbol{\Gamma}(t) \rangle &= 0, \quad \langle \boldsymbol{\Gamma}(t_1) \boldsymbol{\Gamma}^T(t_2) \rangle = 2\text{Pe}^{-1} \mathbb{K} \delta(t_1 - t_2). \end{aligned} \quad (7)$$

Here \mathbb{I} is the moment of inertia of the particle, and the stochastic torque $\boldsymbol{\Gamma}(t)$ represents the torque due to thermal motion in the fluid. The angular brackets $\langle \dots \rangle$ denote an average over thermal noise. The random torque has a very short (molecular) correlation time τ , represented by the correlation function $\delta_\tau(t)$ in Eq. (7), and its statistics are determined by equipartition: the particle must be in thermal equilibrium with the surrounding fluid [22]. One integrates Eq. (7) for a small time step δt , together with the kinematic equation

$$\frac{d}{dt} R_{\alpha i} = \varepsilon_{ijk} \omega_j R_{\alpha k} = -\varepsilon_{\alpha\beta\gamma} \omega_{\beta} R_{\gamma i} \quad (8)$$

that describes the rotation of the particle-orientation vectors \mathbf{n}^β with angular velocity $\boldsymbol{\omega}$. The small time step is assumed to be much smaller than the time over which the distribution of $\mathbb{R}(t)$ changes ($\delta t \ll 1$ for large Pe), yet large compared to the viscous time ($\delta t \gg \text{St}$). In this limit one finds the following expressions for the moments of the particle angular velocity [22]:

$$\int_0^{\delta t} dt \langle \boldsymbol{\omega}(t) \rangle \sim \boldsymbol{\omega}^H \delta t \quad \text{for } \text{St} \ll \delta t \ll 1, \quad (9a)$$

and

$$\int_0^{\delta t} dt_1 \int_0^{\delta t} dt_2 \langle (\boldsymbol{\omega}(t_1) - \boldsymbol{\omega}^H) \cdot (\boldsymbol{\omega}(t_2) - \boldsymbol{\omega}^H) \rangle \sim 2\text{Pe}^{-1} \mathbb{K}^{-1} \delta t \quad \text{for } \text{St} \ll \delta t \ll 1. \quad (9b)$$

TABLE I. The dimensionless elements of the resistance tensors in relation to expressions in Haber and Brenner [19]. A factor of 2 is missing in Eq. [A1] for ${}^r\mathbf{K}$ on p. 510 of Haber and Brenner [19]. We have used the correct expression from Ref. [26].

Notation in this paper	Notation in Ref. [19]	Eqs. in Ref. [19]
\mathbb{K}	$6 {}^r\mathbf{K}$	Eqs. [3.1], [A1]
\mathbb{H}	$6\boldsymbol{\tau}$	Eqs. [3.1], [A2]
\mathbb{Z}	$5\mathbf{Q}$	Eqs. [3.1], [A3], [A4]

The asymptotic form of the integral of the angular-velocity autocorrelation function is consistent with Einstein's argument mentioned above. We note that the minus sign in Eq. (8) arises from transforming the equation of motion to body coordinates. This explains the minus sign in Eq. (6b), written in body coordinates. Finally we remark that the second term on the r.h.s. of Eq. (6b) is a spurious drift term [23]. It arises here because $\frac{d}{dt}\mathbb{R}$ is a non-linear function of \mathbb{R} since $\boldsymbol{\omega}^H$ depends upon the particle orientation through the resistance tensors, and thus on \mathbb{R} . An analogous situation is described in Ref. [24]. Finally, averaging the angular displacements $\delta\mathbb{R}$ at fixed initial orientation one finds, using (9a) and (9b), the Langevin equation (6).

To simulate Eq. (6) in practice, we represent the orientation by a unit quaternion instead of a rotation matrix [25]. The unit quaternion is better than the rotation matrix for numerical computation because it has four scalar components and a unit constraint $|\mathbf{q}| = 1$, whereas the rotation matrix has nine scalar components and the orthogonality constraint $\mathbb{R}^T \cdot \mathbb{R} = \mathbb{1}$. The Langevin equation in quaternion coordinates is described in Appendix B.

C. Dilute suspension rheology

The macroscopic description of a particulate suspension is based on a statistical model of the microscopic fluid mechanics of all the suspended particles [27]. For a sufficiently homogeneous suspension, a macroscopic observable such as the stress tensor $\boldsymbol{\sigma}$, may be represented by an average of the microscopic configurations. In general this averaging is a very complicated task [3]. But for a dilute suspension it is sufficient to consider the stress contribution from an isolated particle and sum the independent contributions from all particles, because particle interactions are negligible. This gives the correct rheology to first order in the volume fraction of particles in the suspension [3, 27].

Batchelor [3] showed that the stress contribution from a single torque-free particle in steady Stokes flow is determined by the symmetric force dipole on the particle, the so-called stresslet. In terms of resistance tensors, the stresslet for a torque-free particle is

$$\mathbb{S} = \mathbb{C} : \mathbb{E}^\infty, \quad (10)$$

where the components of \mathbb{C} are

$$C_{ijkl} = R_{\alpha i} R_{\beta j} R_{\gamma k} R_{\delta l} (Z_{\alpha\beta\gamma\delta} - H_{\mu\alpha\beta} K_{\mu\nu}^{-1} H_{\nu\gamma\delta}). \quad (11)$$

The rank-four tensor \mathbb{Z} is the resistance tensor coupling stresslet and strain (Table I). Eq. (10) was derived by Batchelor [3] in the steady Stokes approximation, assuming weak thermal noise (large Péclet numbers). While the Langevin equation (6) is valid for arbitrary Péclet numbers, *unsteady* fluid inertia might affect the Brownian contribution to the stress for triaxial particles. It may well be, on the other hand, that the steady Stokes approximation is sufficient. To show this one should find an argument – analogous to Einstein's – that shows that the steady Stokes approximation gives the correct result. For a diffusing sphere it is known that the velocity autocorrelation function is wrongly predicted by the steady Stokes approximation, yet the long-time mean squared displacement of the centre-of-mass comes out correctly.

Here we consider the limit of large Péclet numbers, to avoid this question. In this limit the extra stress Σ_p due to the presence of particles in a dilute suspension of volume V is given by [3]

$$\Sigma_p = \frac{V_p}{V} \sum_m \mathbb{S}^{(m)}, \quad (12)$$

where $\mathbb{S}^{(m)}$ denotes the stresslet from the m :th particle and the sum is over all particles. The stresslet (10) depends on the the shape and orientation of the particle. If there are many identical particles in V , the sum over particles

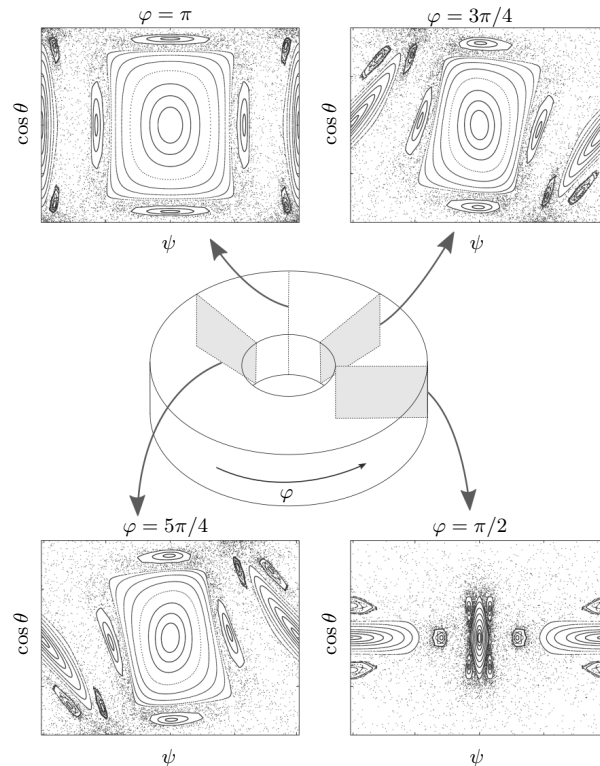


FIG. 2. Schematic explanation of the surfaces-of-section shown in Section III A (for $\lambda = 10$ and $\kappa = 5$). The torus depicts the three-dimensional angular space for an ellipsoid. The major axis of the ellipsoid rotates monotonously around the vorticity [15], depicted by the azimuthal angle φ , see also Fig. 1. The surfaces-of-section shown are for $\varphi = \pi/2 + n\pi/4$, for $n = 0, \dots, 3$, corresponding to four directions of the projection of \mathbf{n}^3 to the flow shear plane: parallel with the flow, of extending strain, perpendicular to the flow, and of compressing strain. The surfaces-of-section for $\varphi \rightarrow \varphi + \pi$ are equal, because the problem is symmetric under this rotation. Figure reproduced from Ref. 29 under the CC-BY 3.0 license.

may be replaced by an angular average over the distribution $P(\mathbb{R})$:

$$\Sigma_p = \phi \int d\mathbb{R} \mathbb{S}(\mathbb{R}) P(\mathbb{R}). \quad (13)$$

Here $\phi = NV_p/V$ is the volume concentration of particles, with N the number of particles in the volume V . The volume concentration is assumed to be small, $\phi \ll 1$. The intrinsic viscosity η is determined by the element $\Sigma_{p;12}$, the shear stress due to the particles [18, 28]:

$$\eta \equiv \frac{1}{\phi} \left(\frac{\mu^*}{\mu} - 1 \right) = \frac{\Sigma_{p;12}}{\phi}. \quad (14)$$

This rheological function depends on the particle shape (λ, κ) and on the value of Pe . When thermal noise is significant there are extra direct Brownian contributions to the stress that we have not considered here. Therefore we only consider the limit of weak thermal noise, corresponding to large values of the Péclet number. In this limit we expect the angular distribution and therefore the intrinsic viscosity to converge to Pe -independent values [12, 13], so that the viscosity becomes independent of Pe , and direct contributions to the stress from Brownian rotation are negligible.

III. NUMERICAL RESULTS

In this Section we show numerical results for the stationary angular distribution and the resulting intrinsic viscosity.

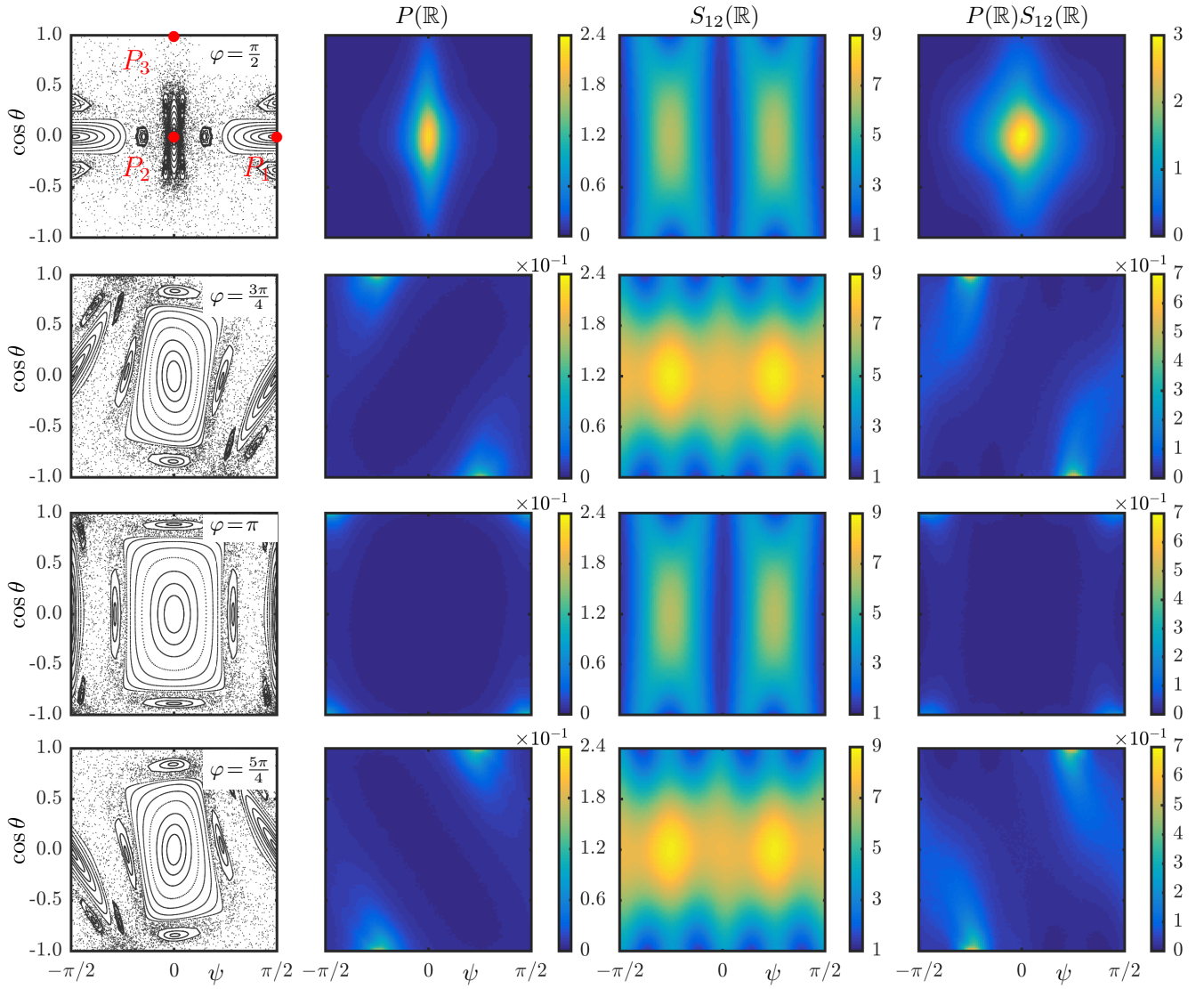


FIG. 3. Rows: four representative surfaces-of-sections for $\varphi = \pi/2 + n\pi/4$, for $n=0, \dots, 3$. These sections correspond to four directions of the projection of \mathbf{n}^3 to the flow shear plane: parallel with the flow, of extending strain, perpendicular to the flow, and of compressing strain (Fig. 2). Columns: (1) the surface-of-section of deterministic trajectories; (2) the stationary angular distributions; (3) the stresslet element corresponding to the intrinsic viscosity of a dilute suspension; (4) the contribution to intrinsic viscosity, given by the product of the angular distribution and the stresslet element. Parameters: $\lambda = 10$, $\kappa = 5$, and $Pe = 200$. The points P_i indicate the locations of three periodic orbits with \mathbf{n}^i parallel to vorticity, for $i = 1, \dots, 3$ (see text).

A. Orientational distributions

The angular trajectories and distributions of a rigid body are difficult to visualize, because they are defined in the three-dimensional non-Euclidean orientation space. But in a particular Euler-angle representation (φ, θ, ψ) (see Appendix B) Hinch and Leal [15] found that $\dot{\varphi} < 0$ in absence of noise. This means that the particle monotonously rotates around the vorticity axis. Therefore it is helpful to think about the orientation space as a torus, in which the deterministic trajectories go around, see Fig. 2. Each transversal slice of constant φ of this torus is a Poincaré surface-of-section [30], schematically shown in Fig. 2. To illustrate the angular distributions, we choose the four representative surfaces-of-sections for $\varphi = \pi/2 + n\pi/4$, for $n=0, \dots, 3$, corresponding to four directions of the projection of \mathbf{n}^3 to the flow shear plane: parallel with the flow, of extending strain, perpendicular to the flow, and of compressing strain (Fig. 2). The first columns of Figs. 3 and 4 show these four surfaces of section for two particle shapes: Fig. 3 is for a strongly triaxial ellipsoid with aspect ratios $\lambda = 10$ and $\kappa = 5$, while Fig. 4 is for a moderately triaxial particle with $\lambda = 10$ and $\kappa = 2$. To obtain these plots we simulated the deterministic angular dynamics (at $Pe = \infty$) and

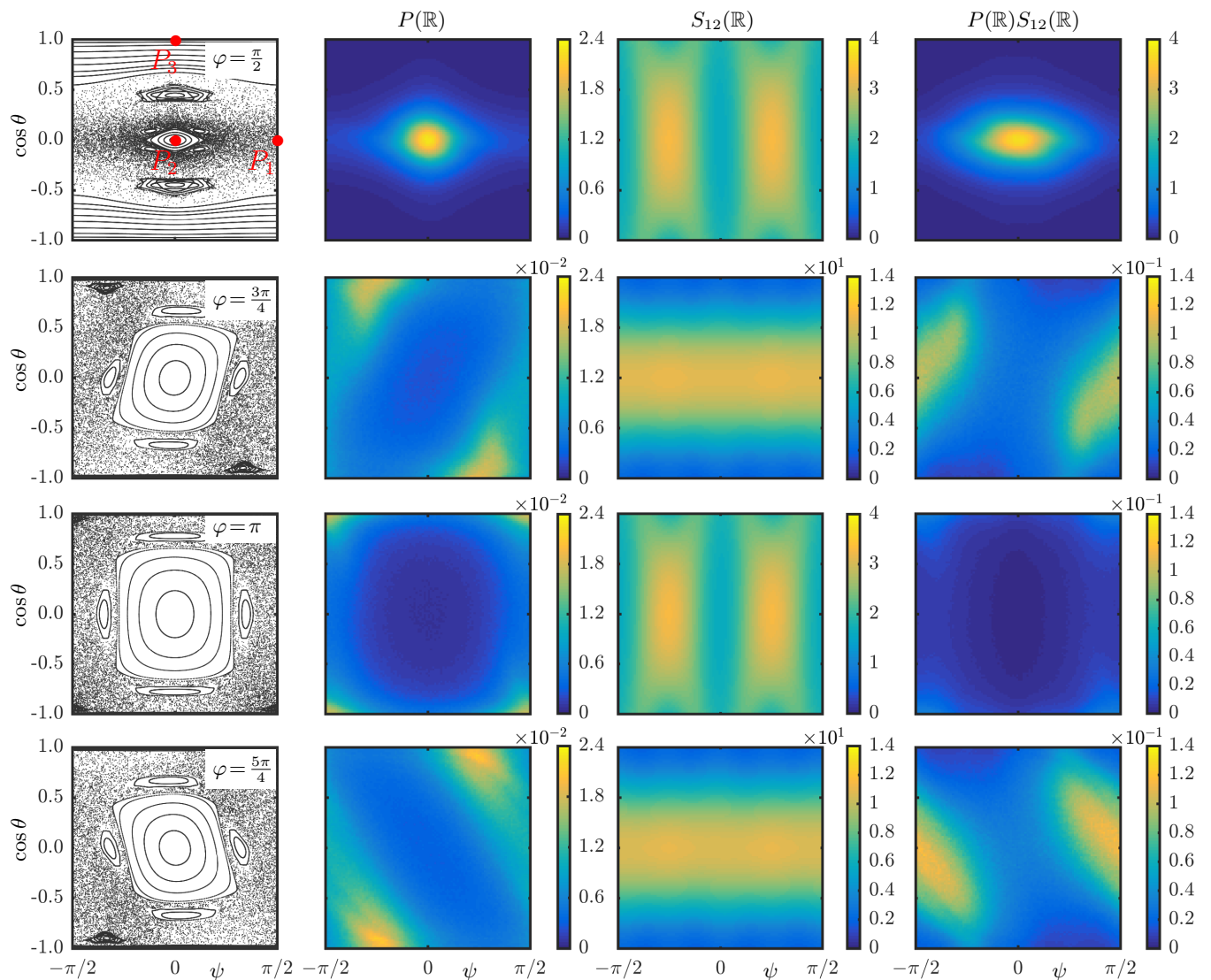


FIG. 4. Rows: four representative surfaces-of-sections for $\varphi = \pi/2 + n\pi/4$, $n = 0..3$, corresponding to four directions of the projection of \mathbf{n}^3 to the flow shear plane: parallel with the flow, of extending strain, perpendicular to the flow, and of compressing strain (Fig. 2). Columns: (1) the surface-of-section of deterministic trajectories; (2) the stationary angular distributions; (3) the stresslet element corresponding to the intrinsic viscosity of a dilute suspension; (4) the contribution to intrinsic viscosity, given by the product of the angular distribution and the stresslet element. Parameters: $\lambda = 10$, $\kappa = 2$, and $\text{Pe} = 200$. The points P_i indicate the locations of three periodic orbits with \mathbf{n}^i parallel to vorticity, for $i = 1, \dots, 3$ (see text).

verified that the integration step size δt was small enough not to affect the results shown. We note that the surfaces of Section in Refs. [15–17] are for $\varphi = n\pi$ (\mathbf{n}^3 perpendicular to the flow).

Another way of visualising the deterministic angular dynamics is to analyse its periodic solutions. Yarin *et al.* [16] described three periodic orbits that correspond to the rotation of the triaxial ellipsoid around \mathbf{n}^1 , \mathbf{n}^2 , and \mathbf{n}^3 . The points P_i in Figs. 3 and 4 indicate where these periodic orbits (\mathbf{n}^i parallel to vorticity) intersect the surfaces-of-section.

Now consider the stochastic angular dynamics. We show distributions of \mathbb{R} for $\lambda = 10$ and $\kappa = 2, 5$ at weak noise ($\text{Pe} = 200$). We verified our numerical algorithm for computing these distributions by evaluating different moments for axisymmetric particles, and found them to be in good agreement with the results of Ref. [12, 18] and [31]. This criterion does not test the far tails of the distributions which are difficult to calculate with high accuracy at large Péclet numbers. Therefore we chose a relatively small value of Pe here, about 10 times smaller than the values used for calculating the intrinsic viscosity (Section III B).

The second columns in Figs. 3 and 4 show our results for the stationary angular distributions. The third columns show the stresslet element corresponding to the intrinsic viscosity of a dilute suspension. In the fourth columns we

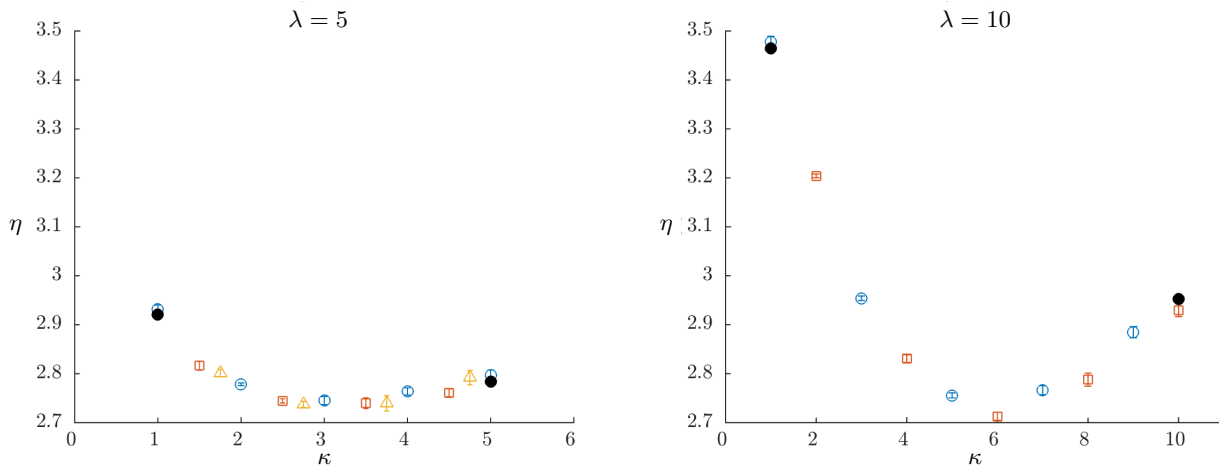


FIG. 5. Intrinsic viscosity of a dilute suspension of triaxial ellipsoids as a function of κ . Left $\lambda = 5$, $Pe = 500$ (\circ), $Pe = 1000$ (\square), $Pe = 2000$ (\triangle). Right: $\lambda = 10$, $Pe = 2000$ (\circ), $Pe = 3000$ (\square). The error bars represent one standard deviation in our average over 200 independent realisations of the Langevin process (6). On the x -axis, the shapes represented by the κ -values range from rods ($\kappa = 1$) to disks ($\kappa = \lambda$). Known limiting values for axisymmetric particles (\bullet) are taken from Refs. [12, 13].

plot the contribution to intrinsic viscosity, given by the product of the angular distribution and the stresslet element. At low thermal noise the distribution is dominated by the deterministic dynamics, and the only effect of the noise is to establish a distribution over the deterministic trajectories. For strong thermal noise, by contrast, the distribution $P(\mathbb{R})$ is nearly isotropic (not shown).

B. Intrinsic viscosity

From Eq. (14) we computed the intrinsic viscosity in the limit of weak thermal noise, at large Péclet numbers. We chose Pe as large as practically possible, so that the intrinsic viscosity converges to a Pe -independent plateau, as in the axisymmetric case [12, 13]. Fig. 5 shows the results for spheroidal particles, for $\lambda = 5$ and 10 as a function of κ . For the data shown we simulated $N = 200$ independent instances of the Langevin equation (B5) for $5 \cdot 10^5$ dimensionless time units, with timesteps δt between 10^{-4} and 10^{-5} . The error bars in Fig. 5 represent one standard deviation in our average over the 200 independent realisations.

In Fig. 5, the parameter κ ranges from $\kappa = 1$ to $\kappa = \lambda$. The limiting cases correspond to rotationally symmetric, ellipsoidal particles. In these special cases our numerical results agree with those of previous work. The values for $\lambda = 10$ and $\kappa = 1, 10$ are determined from Eq. (27) in [13], together with the angular averages from Table 1 in this paper. The angular averages for $\lambda = 5$ and $\kappa = 1, 5$ are taken from Table 3 in [12]. For the $\lambda = 10$ -particle slightly higher Pe -values are needed to obtain this convergence than for the $\lambda = 5$ -particle. We observe good agreement with these results for axisymmetric particles (to within a fraction of a percent), but the agreement is not perfect. We checked that the remaining error is not due to the finite integration step size δt by varying this step size. A possible source of error is the statistical error due to finite sample size, and we cannot rule out that the initial transient may result in a small systematic error.

IV. DISCUSSION

A. Orientational distributions

The deterministic angular trajectories depend very sensitively on the shape of the particle. While axisymmetric ellipsoids tumble on periodic Jeffery orbits, a slight breaking of this symmetry can lead to doubly periodic, and even chaotic angular dynamics [15–17], as the the surfaces-of-section in the first rows of Figs. 3 and 4 show. The closed concentric lines near $\cos \theta = 0$ in these surfaces-of-section describe doubly-periodic tumbling, while the black regions correspond to chaotic tumbling. The almost horizontal lines near $|\cos \theta| = 1$ correspond to slightly perturbed Jeffery orbits (log rolling).

The surfaces-of-section look very similar to those of Hamiltonian dynamics [30]. This may appear surprising, because our dynamics is dissipative, not Hamiltonian. But it is no coincidence that the surfaces-of-section look so similar. While our system does not conserve energy, it is time-reversal invariant and exhibits a discrete reflection symmetry [17] that constrains the angular dynamics in a way analogous to the symplectic structure of Hamiltonian dynamics [30, 32].

For weak noise, the particle orientation tends to follow deterministic trajectories, but occasionally jumps to a neighboring trajectory. This process establishes an equilibrium distribution of the particle orientation over the deterministic trajectories after some time. Which orientations are most probable, and how does the distribution reflect the nature of the deterministic angular dynamics?

Figs. 3 and 4 show that the probability is highest in the flow-shear plane, when \mathbf{n}^3 aligns with the flow direction (first rows of Figs. 3 and 4). This is simply a consequence of the time-scale separation in the deterministic dynamics when λ is not near 1: elongated particles spend most of their time aligned with the flow where the angular dynamics is slow. This orientation corresponds to a local minimum of shear stress (third panel in first row of Figs. 3 and 4).

The other three surfaces of section capture how the angular dynamics when the projection of \mathbf{n}^3 is not aligned with the flow direction. The probability is not uniformly distributed over the surfaces of section. Also in this case peaks in $P(\mathbb{R})$ are explained by slow angular dynamics. Consider the second row of Figs. 3 and 4, corresponding to $\varphi = 3\pi/4$. The probability is peaked at $(\cos\theta, \psi) \approx (1, -\pi/4)$ and the symmetric point $(-1, \pi/4)$. The condition $\cos\theta = \pm 1$ corresponds to the log-rolling orbit, and when $\cos\theta = 1$ then $\psi = -\pi/4$ ensures that the short axis \mathbf{n}^1 aligns with the shear direction where the shear-induced torque $\mathbb{H} : \mathbb{E}^\infty$ is minimal, so that the angular dynamics is slow. The same argument holds for $\cos\theta = -1$ then $\psi = \pi/4$. In rows 3 and 4 of Figs. 3 and 4 the situation is analogous: the probability $P(\mathbb{R})$ is largest for orientations where the shear-induced torque is smallest. Comparing Figs. 3 and 4 we see that the maximal values of $P(\mathbb{R})$ are similar (first rows). This is expected because the parameter λ is the same. The probability in rows 2, 3, and 4 is larger in Fig. 3 ($\kappa = 5$) compared with Fig. 4 ($\kappa = 2$). A larger value of κ corresponds to slower dynamics, and thus to higher probability. In summary, the probability $P(\mathbb{R})$ of orientations in the weak-noise limit is strongly peaked where the deterministic dynamics is slowest, regardless of whether it is periodic, doubly periodic or possibly chaotic.

B. Intrinsic viscosity

The orientation-dependent contribution to intrinsic viscosity $S_{12}(\mathbb{R})$, however, has a local minimum where the probability density is concentrated (Figs. 3 and 4). Nevertheless, this direction dominates the contribution to the intrinsic viscosity at weak noise. With the major axis along the flow direction, the orientation corresponding to maximal shear stress is when the particle is tilted 45° . Although those particle orientations are relatively unlikely, they contribute to the integral of $P(\mathbb{R})S_{12}(\mathbb{R})$ because of their relatively high shear stress.

Fig. 5 shows the resulting intrinsic viscosity. We see that Pe is large enough so that the intrinsic viscosity is approximately independent of Pe , to within numerical accuracy. For the $\lambda=10$ -particle slightly higher Pe -values are needed to obtain this convergence, than for the $\lambda=5$ -particle. We believe this is because the effective Pe in regions of slow deterministic dynamics is actually smaller than the naive estimate $\text{Pe} = s/D$ and the more elongated the particle is, the slower is the dynamics in such regions [12].

For all particle shapes shown the intrinsic viscosity is larger than that of spheres ($\eta = 5/2$). This is consistent with the observation that the intrinsic viscosity of a dilute suspensions of axisymmetric particles increases with larger particle aspect ratio [12], most strongly for suspensions of prolate particles. The effect of making the particles triaxial, however, is to decrease the resulting intrinsic viscosity, as can be seen in Fig. 5. The Figure shows that the intrinsic viscosity depends only weakly on κ , except for rod-like axisymmetric particles. We conclude that the intrinsic viscosity does not depend as sensitively on particle shape as the deterministic angular dynamics, even at low thermal noise where the angular dynamics follows deterministic trajectories for long times. Figs. 3 and 4 show that this is the consequence of two effects. First, the angular dynamics is most sensitive to particle shape near orientations where the particle spends least time. Second, the additional stress caused by the particle is comparatively small at these orientations.

To illustrate these conclusions in a different way, we computed the intrinsic viscosities associated with the three periodic orbits mentioned above, where the triaxial ellipsoid rotates about one of its major axes, \mathbf{n}^i for $i = 1, \dots, 3$. The first orbit (P_1 in Figs. 3 and 4) corresponds to a particle rotating with its small axis parallel to the undisturbed vorticity Ω^∞ , P_2 to rotation with the intermediate axis parallel to vorticity, and P_3 to rotation with the long axis parallel to vorticity. For each orbit we averaged S_{12} [Eq. (14)] along the orbit. The results are shown in Fig. 6. We see that the orbit corresponding to P_1 is the most dissipative one: if all particles rotated with their small axis parallel to vorticity, the intrinsic viscosity would reach large values. However, this orbit is known to be unstable [16], and has a low probability in the weak-noise dynamics (see Figs. 3 and 4). The orbit corresponding to P_2 (medium axis parallel

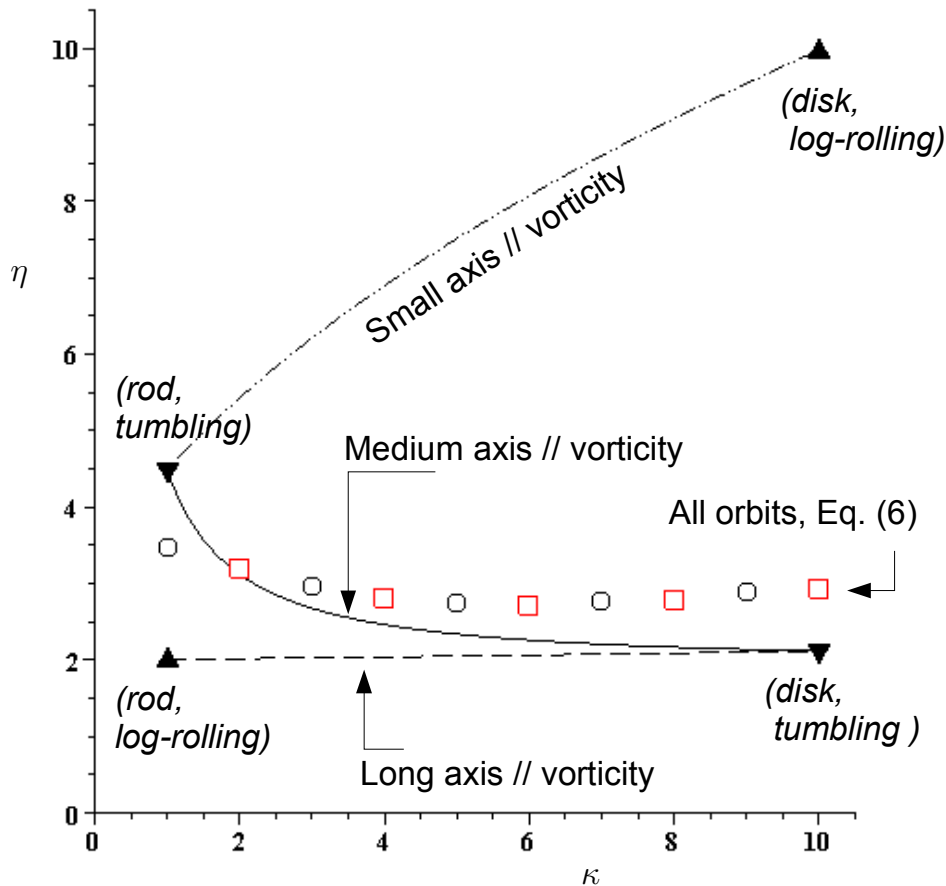


FIG. 6. Plot of the intrinsic viscosities for the three periodic orbits corresponding to rotation with one axis parallel to vorticity (see text), as a function of κ for $\lambda = 10$. Solid line: intermediate axis parallel to vorticity, dashed line: long axis parallel to vorticity, dot-dashed line: short axis parallel to vorticity. Triangles correspond to values for axisymmetric particle that were computed by Jeffery [4]: tumbling (\blacktriangledown) and log rolling (\blacktriangle). Squares and circles are the numerical data from Fig. 5 (right), for Péclet number equal to 2000 (circles) and 3000 (squares).

to vorticity), by contrast, has the highest probability of the three periodic orbits in the weak-noise dynamics, as Figs. 3 and 4 show. It is much less dissipative though. This suggests that particles spend a long time with medium axis aligned with vorticity in the weak-noise limit, and that this yields the dominant contribution to the overall intrinsic viscosity of the dilute suspension.

V. CONCLUSIONS

We analyzed the angular dynamics of triaxial ellipsoids in a shear flow subject to weak thermal noise (large Péclet numbers). By numerically integrating the corresponding angular Langevin equation, we found the stationary probability distribution for a range of asymmetric particle shapes at weak thermal noise. We showed that the probability is largest when the deterministic angular dynamics is slow, regardless of whether it is strictly periodic, doubly periodic, or chaotic.

We also compared how the angular distribution correlates with the orientation-dependent contribution to the intrinsic viscosity of a dilute suspension. We found that the angular probability is concentrated in a local minimum of the shear stress. In general though the shear stress is much less localized than the angular probability.

Finally, we computed the intrinsic viscosity of a dilute suspension of triaxial ellipsoids at weak noise, and found that the intrinsic viscosity decreases as particles deviate from axisymmetric shape (for particles with the same volume, and with the same ratio of major to minor axis lengths). This effect is strongest for rod-shaped particles, it is thus important to ensure that rod-like particles are axisymmetric to high precision when trying to achieve a maximal increase in suspension viscosity by adding rod-like particles to a suspension. For example, at $\lambda = 10$ changing κ from 1 to 2 gives a 10%-reduction in intrinsic viscosity. In general, however, we found that the dependence of the intrinsic

viscosity on particle shape is much less sensitive than the nature of the deterministic angular dynamics, because the angular probability is localized where the shear-induced torque is small, regardless of the nature of the classical dynamics.

Finally, at lower values of Pe , suspensions of spheroids exhibit normal stress differences [12] that are $O(Pe^{-1})$ smaller than the shear-stress correction, and therefore outside the scope of the present study. Computing the rheological properties of suspensions of triaxial particles at lower values of Pe is an interesting future research opportunity.

ACKNOWLEDGMENTS

We thank K. Kroy for discussions. We acknowledge support by Vetenskapsrådet [grant numbers 2013-3992 and 2017-3865], by the grant ‘Bottlenecks for particle growth in turbulent aerosols’ from the Knut and Alice Wallenberg Foundation, Dnr. KAW 2014.0048, and by the MPNS COST Action MP1305 ‘Flowing matter’. The numerical computations used resources provided by C3SE and SNIC.

-
- [1] A. Einstein, “Eine neue Bestimmung der Moleküldimensionen,” *Ann. Phys.* **324**, 289–306 (1906).
 - [2] A. Einstein, “Berichtigung zu meiner Arbeit: „Eine neue Bestimmung der Moleküldimensionen”,” *Ann. Phys.* **339**, 591–592 (1911).
 - [3] G. K. Batchelor, “The stress system in a suspension of force-free particles,” *J. Fluid Mech.* **41**, 545–570 (1970).
 - [4] G. B. Jeffery, “The Motion of Ellipsoidal Particles Immersed in a Viscous Fluid,” *Proc. R. Soc. A* **102**, 161–179 (1922).
 - [5] P. G. Saffman, “On the motion of small spheroidal particles in a viscous liquid,” *J. Fluid Mech.* **1**, 540 (1956).
 - [6] E. Y. Harper and I-Dee Chang, “Maximum dissipation resulting from lift in a slow viscous shear flow,” *J. Fluid Mech.* **33**, 209–225 (1968).
 - [7] G. Subramanian and D. L. Koch, “Inertial effects on fibre motion in simple shear flow,” *J. Fluid Mech.* **535**, 383–414 (2005).
 - [8] J. Einarsson, F. Candelier, F. Lundell, J. R. Angilella, and B. Mehlig, “Effect of weak fluid inertia upon Jeffery orbits,” *Phys. Rev. E* **91**, 041002 (2015).
 - [9] J. Einarsson, F. Candelier, F. Lundell, J. R. Angilella, and B. Mehlig, “Rotation of a spheroid in a simple shear at small Reynolds number,” *Phys. Fluids* (1994-present) **27**, 063301 (2015).
 - [10] T. Rosen, J. Einarsson, A. Nordmark, C. K. Aidun, F. Lundell, and B. Mehlig, “Numerical analysis of the angular motion of a neutrally buoyant spheroid in shear flow at small Reynolds numbers,” *Phys. Rev. E* **92**, 063022 (2015).
 - [11] Howard Brenner, “Orientation-space boundary layers in problems of rotational diffusion and convection at large rotary Péclet numbers,” *J. Colloid Interface Sci.* **34**, 103–125 (1970).
 - [12] E. J. Hinch and L. G. Leal, “The effect of Brownian motion on the rheological properties of a suspension of non-spherical particles,” *J. Fluid Mech.* **52**, 683–712 (1972).
 - [13] L. G. Leal and E. J. Hinch, “The effect of weak Brownian rotations on particles in a shear flow,” *J. Fluid Mech.* **46**, 685–703 (1971).
 - [14] P. J. Gierszewski and C. E. Chaffey, “Rotation of an isolated triaxial ellipsoid suspended in slow viscous flow,” *Can. J. Phys.* **56**, 6–11 (1978).
 - [15] E. J. Hinch and L. G. Leal, “Rotation of small non-axisymmetric particles in a simple shear flow,” *J. Fluid Mech.* **92**, 591–608 (1979).
 - [16] A. L. Yarin, O. Gottlieb, and I. V. Roisman, “Chaotic rotation of triaxial ellipsoids in simple shear flow,” *J. Fluid Mech.* **340**, 83–100 (1997).
 - [17] J. Einarsson, B. Mihiretie, A. Laas, S. Ankardal, J. R. Angilella, D. Hanstorp, and B. Mehlig, “Tumbling of asymmetric microrods in a microchannel flow,” *Phys. Fluids* **28**, 013302 (2016).
 - [18] J. M. Rallison, “The effects of Brownian rotations in a dilute suspension of rigid particles of arbitrary shape,” *J. Fluid Mech.* **84**, 237–263 (1978).
 - [19] S. Haber and H. Brenner, “Rheological properties of dilute suspensions of centrally symmetric Brownian particles at small shear rates,” *J. Colloid Interface Sci.* **97**, 496–514 (1984).
 - [20] H. Goldstein, *Classical Mechanics* (Addison-Wesley, Reading, Massachusetts, 1980).
 - [21] G. Bossis and J. F. Brady, “The rheology of Brownian suspensions,” *J. Chem. Phys.* **91**, 1866 (1989).
 - [22] F. Perrin, “Mouvement Brownien d’un ellipsoïde (I). Dispersion diélectrique pour des molécules ellipsoïdales,” *J. Phys. Radium* **5**, 497–511 (1934).
 - [23] N. G. Van Kampen, *Stochastic Processes in Physics and Chemistry* (Elsevier Science Publishers, 1981).
 - [24] B. Mehlig, M. Wilkinson, K. Duncan, T. Weber, and M. Ljunggren, “Aggregation of inertial particles in random flows,” *Phys. Rev. E* **72** (2005), 051104.
 - [25] B. Graf, “Quaternions and dynamics,” arXiv:0811.2889 [math-ph] (2008).
 - [26] Sangtae Kim and Seppo J. Karrila, *Microhydrodynamics: principles and selected applications*, Butterworth-Heinemann series in Chemical Engineering (Butterworth-Heinemann, Boston, 1991).

- [27] H. Brenner, “Suspension Rheology,” in *Prog. Heat Mass Transf.* (Pergamon, 1972) pp. 89–129.
- [28] H.W. Giesekus, “Elasto-viskose Flüssigkeiten, für die in stationären Schichtströmungen sämtliche Normalspannungskomponenten verschieden groß sind,” *Rheol. Acta* **2**, 50–62 (1962).
- [29] J. Einarsson, *Angular dynamics of small particles in fluids*, PhD thesis, University of Gothenburg (2015).
- [30] S. H. Strogatz, *Nonlinear dynamics and Chaos* (Westview Press, 1994).
- [31] J. Einarsson, J. R. Angilella, and B. Mehlig, “Orientational dynamics of weakly inertial axisymmetric particles in steady viscous flows,” *Physica D* **278**, 79 (2014).
- [32] A. Politi, G. L. Oppo, and R. Badii, “Coexistence of conservative and dissipative behavior in reversible dynamical systems,” *Phys. Rev. A* **33**, 4055–4060 (1986).

Appendix A: Euler angles

In this appendix we describe how we parameterize the rotation matrix \mathbb{R} in terms of Euler angles. We use Euler angle coordinates in the Goldstein z - x' - z'' convention [20]: starting from $\mathbf{n}^i = \mathbf{e}^i$, first rotate the \mathbf{n}^i by φ around \mathbf{n}^3 , then by θ around the resulting \mathbf{n}^1 and finally by ψ around the resulting \mathbf{n}^3 , compare Fig. 1 in the main text and Fig. 4-7 in Ref. [20]. With the shorthand $cx = \cos x$ and $sx = \sin x$ the elements of the rotation matrix are

$$\mathbb{R} = \begin{pmatrix} c\varphi c\psi - \theta s\varphi s\psi & c\psi s\varphi + \theta c\varphi s\psi & s\theta s\psi \\ -\theta c\psi s\varphi - c\varphi s\psi & \theta c\varphi c\psi - s\varphi s\psi & c\psi s\theta \\ s\theta s\varphi & -c\varphi s\theta & c\theta \end{pmatrix}. \quad (\text{A1})$$

Evaluating the determinant we can confirm that \mathbb{R} is orthogonal. Our convention is the same as that adopted in Ref. [15], and Fig. 1 in their paper corresponds to our Fig. 1. Our axis \mathbf{n}^3 corresponds to their z' -axis.

Appendix B: Quaternion formulation of the Langevin equation, Eq. (6)

In this appendix we describe how the Langevin equations (6) are expressed in terms of quaternions. Our quaternion description follows that of Graf [25]. Here we give the practical details relevant for simulation of the Langevin equation (6). We represent the unit quaternion q as a four-component unit vector $\mathbf{q} = (W, X, Y, Z)$, $|\mathbf{q}| = 1$. Its relation to the rotation matrix \mathbb{R} is

$$\mathbb{R} = \mathbb{E} \cdot \mathbb{G}^T, \quad (\text{B1})$$

where

$$\mathbb{E} = \begin{pmatrix} -X & W & -Z & Y \\ -Y & Z & W & -X \\ -Z & -Y & X & W \end{pmatrix}, \quad (\text{B2})$$

$$\mathbb{G} = \begin{pmatrix} -X & W & Z & -Y \\ -Y & -Z & W & X \\ -Z & Y & -X & W \end{pmatrix}. \quad (\text{B3})$$

The equation of motion of \mathbf{q} corresponding to Eq. (8) is given in Ref. [25]:

$$\dot{q}_i = \frac{1}{2} G_{\alpha i} \omega_\alpha, \quad (\text{B4})$$

where $\boldsymbol{\omega}$ is the angular velocity of the particle in body coordinates. Using Eqs. (9a) and (9b) we derive

$$q_i(t + \delta t) = q_i(t) + \delta q(t) \quad (\text{B5a})$$

$$\overline{\delta q}_i = \frac{1}{2} G_{\alpha i} \omega_\alpha^H \delta t - \frac{1}{4} \text{Pe}^{-1} K_{\alpha\alpha}^{-1} q_i \delta t + \mathcal{O}(\delta t^2), \quad (\text{B5b})$$

$$\overline{\delta q}_i \overline{\delta q}_j = \frac{1}{2} \text{Pe}^{-1} G_{\alpha i} K_{\alpha\beta}^{-1} G_{\beta j} \delta t + \mathcal{O}(\delta t^2). \quad (\text{B5c})$$

This Langevin equation is equivalent to Eq. (6) in the main text.